Bollettino di Geofisica Teorica ed Applicata Vol. 52, n. 2, pp. x-xx; June 2011
DOI 10.4430/bgta0006

Assessment of errors from different electrode materials and configurations for electrical resistivity and time-domain IP data on laboratory models

G. De Donno and E. Cardarelli

Dip. Ingegneria Civile Edile Ambientale, Università La Sapienza, Roma, Italy

(Received: July 16, 2010; accepted: December 23, 2010)

ABSTRACT In the last twenty years Electrical Resistivity Tomography and time-domain Induced Polarization techniques have been widely used for geological, environmental, chemical and hydro-geological applications. As a matter of fact, the choice of electrodes (material and number) to be employed is crucial to avoid large measurement errors. The aim of this work is the quantitative assessment of errors in acquisition with respect to different electrode materials and configurations, as well as a comparison with previous results. To this end, a cylindrical column (height of 280 mm, diameter of 135 mm) is set up and all measurements are performed on a 7 electrode, 2D horizontal cross-section. Resistance, chargeability and self-potential measurements for different electrode materials (steel, iron, aluminium, copper and carbon) are acquired over a cylindrical sample filled by water with known conductivity. A statistical analysis of the experimental data demonstrates that iron and steel provide the best performances both for resistance and for chargeability. Carbon and copper are reliable for resistive surveys, but not for capacitive ones. Standard deviations associated to aluminium electrodes are the highest among the five materials. Changing the number of electrodes (from 7 to 20) results in an exponential increase of resolution of the resistive and chargeable anomalies included in the samples.

Key words: acquisition errors, electrodes, ERT.

1. Introduction

A suitable choice of electrodes is crucial for geo-electrical surveys due to important differences in the material response to an electrical impulse. As a matter of fact, part of the measured signal on the potential electrodes depends on electrochemical phenomena at the contact point between the electrolyte and the electrode (Vanhala and Soininen, 1995; Dahlin *et al.,* 2002; La Brecque and Daily, 2008) and on a charge-up effect due to a previous use as a current electrode (Dahlin, 2000). Since the latter effect can be avoided via a plus-minus-plus measurement cycle and a suitable sequence (Dahlin *et al.,* 2002), the electrochemical polarization acts as a primary source of errors, particularly for chargeability data.

During the last decade, different electrode materials have been employed for Electrical Resistivity Tomography (ERT) and Induced Polarization (IP) surveys, performed in the field and at laboratory scale: steel (Weller *et al.,* 1999; Dahlin, 2000; Slater and Glaser, 2003; Hordt *et al.,* 2007), copper, mainly for current-carrying electrodes (Titov *et al.,* 2004; Cardarelli and Di

© 2011 – OGS

Filippo, 2009) gold-plated (Vanhala and Soininen, 1995) and silver-plated (Slater *et al.,* 2005), platinum (Vanhala and Soininen, 1995), non-polarisable Ag-AgCl (Slater *et al.,* 2005), Pb-$PbCl_2$ (Dahlin *et al.,* 2002) and Cu-$CuSO_4$, only as potential electrodes. Carbon electrodes are often used for electrokinetic remediation laboratory studies (e.g., Acar *et al.,* 1995), due to their low cost compared with noble metals.

Dahlin *et al.* (2002) made a quantitative comparison between steel and Pb/$PbCl_2$ electrodes, demonstrating the possibility of reducing errors associated to steel electrodes using efficient field procedures. La Brecque and Daily (2008) performed AC resistivity and chargeability measurements among fourteen different materials, stressing the weight of errors due to electrochemical polarisation. Nevertheless, these results need further investigation to evaluate electrode performances for DC sources and to confirm previous evidence. In this sense, one can restrict the analysis to the most widely-used materials (steel, iron, aluminium, carbon and copper).

Another critical aspect for laboratory surveys on cylindrical samples is the number of electrodes employed to achieve a sufficient resolution of the physical anomalies. Wheeler *et al.* (2002) have studied angular, radial and areal resolutions, introducing a couple of indices to evaluate the spatial resolution in image reconstruction. A set of reference criteria was elaborated by Adler *et al.* (2009).

Our aim is to improve these results, including the chargeability data and assessing resolution achieved by different electrode configurations.

In the light of this, the main goals of this work are:

- to assess the errors due to different electrode materials (steel, iron, copper, carbon and aluminium), arising during laboratory time-domain DC geo-electrical surveys performed by a multichannel instrument;
- to discuss a quantitative comparison for the results after La Brecque and Daily (2008);
- to evaluate the effect of the number of electrodes for reconstruction of resistive and chargeable inclusions within a cylindrical model.

2. Experimental set-up

Laboratory experiments are performed over a cylindrical PVC test-column (height H = 280 mm, diameter ϕ = 135 mm), shown in Fig. 1. A horizontal mid-section is provided, with 7 electrodes having a diameter of 3 mm. The column is saturated with tap water having a known resistivity ρ (17÷20 Ω·m, depending on temperature).

As cited above, the five materials analyzed are: steel (no stainless), iron, copper, aluminium and carbon. Preliminarily, Self Potential (SP) measurements were performed, using an ABEM Terrameter instrument, for 60 minutes after the water spilling (t_0), in order to estimate the effect of noise due to thermal disequilibrium. In Fig. 2, SP time-histories for aluminium electrodes (displaying the highest SP values among the five materials) are represented for three different dipoles (located between electrodes 1 and 2, 1 and 3, and 1 and 4, in Fig. 1). SP values become lower than 5 mV, 35-40 minutes after t_0. Resistance and chargeability measurements were then performed with a multichannel resistivimeter Syscal Pro 48 by IRIS instruments. Using this type of instrument avoids having the charge-up effect on the potential electrodes, because of the plus-

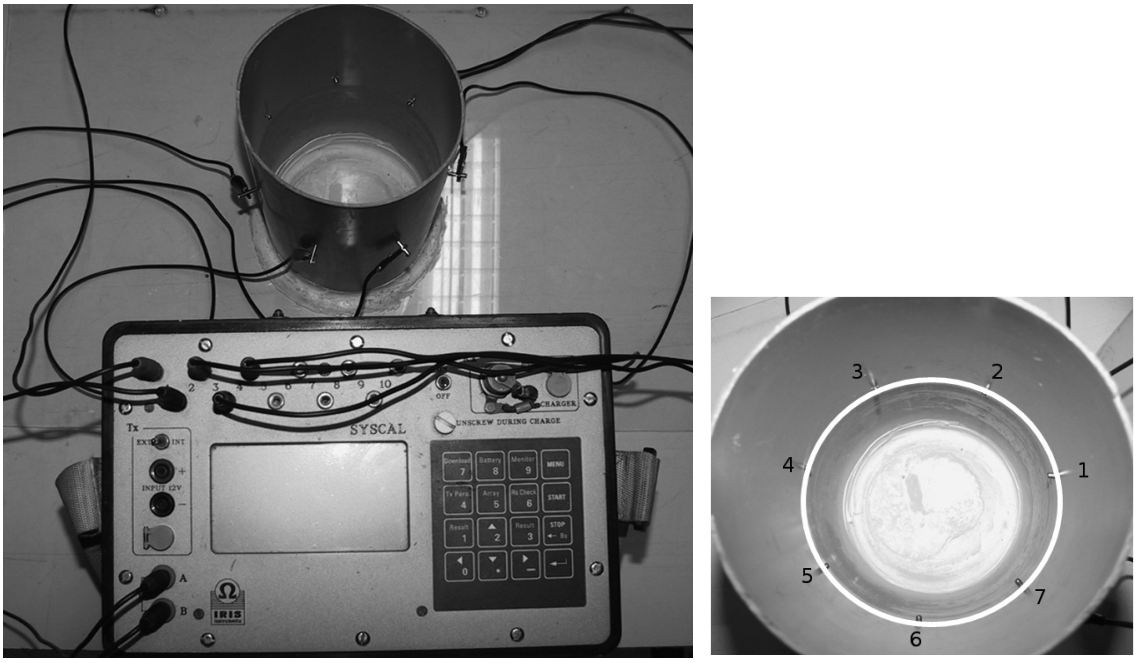

Fig. 1 - Experimental cylindrical PVC device and IRIS Syscal Pro resistivimeter (left). Top view with horizontal mid-section and electrodes highlighted (right).

minus-plus type of input signal. Resistance measurements are performed using a current injection time equal to 1 s, with a 12 V maximum amplitude of the input signal. The chargeability decay curve (Fig. 3) is defined by a semi-logarithmic sampling, using 20 IP windows. The acquisition parameters are summarized in Table 1.

From an L electrodes configuration, $L \cdot (L\text{-}3)$ measurements (28 in this case) can be carried out

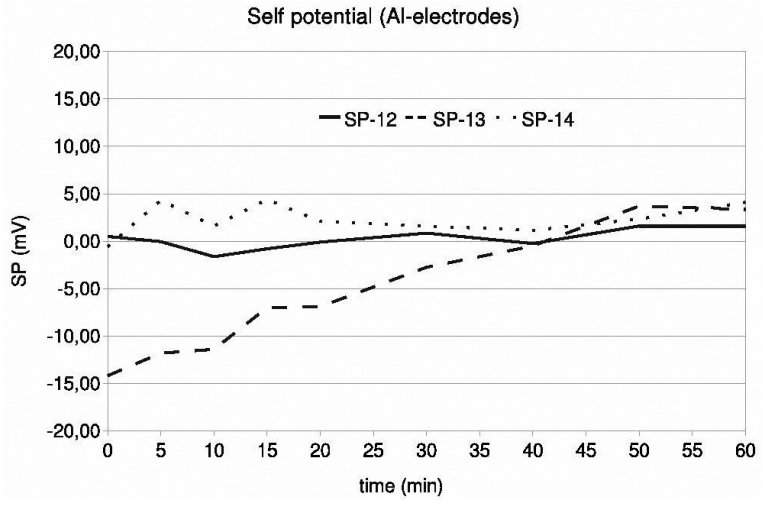

Fig. 2 - SP measurements performed on aluminium electrodes for 60 minutes after water spilling. Three examples SP 1-2, SP 1-3, SP 1-4 are represented by solid, dashed and dotted lines respectively.

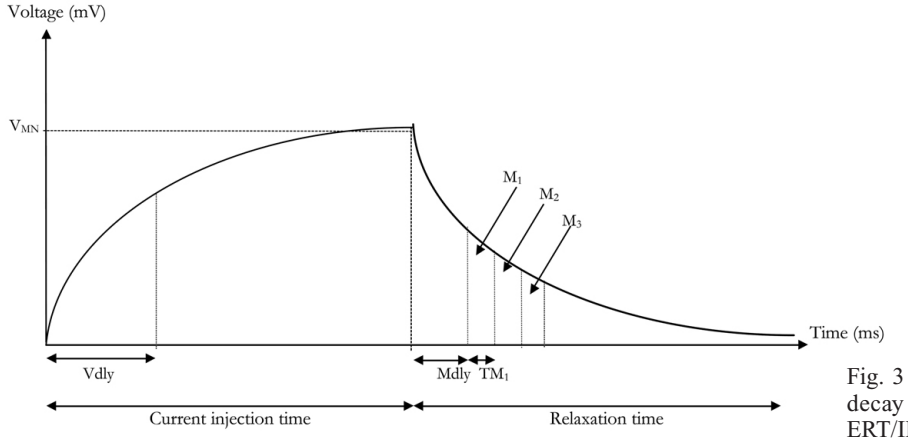

Fig. 3 - Current injection and decay curve for a typical ERT/IP survey.

using an adjacent dipole-dipole array (Fig. 4) and only $L\cdot(L\text{-}3)/2$ using reciprocal pairs (14 in this case).

To by-pass this problem and enlarge the data set, 8 cycles were stacked for each measurement of resistance and chargeability (224 values).

A reciprocal measurement pair is defined as a four-electrode resistance measurement (R_i) along with a resistance measurement after interchanging the current source and the voltage-sensing dipoles (R_{-i}) (La Brecque and Daily, 2008). Using reciprocal measurements, errors are less likely to be correlated than would be the case with simple repeated measurements (La Brecque and Daily, 2008). Therefore, the resistance data set is analyzed as Resistance Difference Error (*RDE*):

$$RDE(\%) = \frac{R_i - R_{-i}}{\bar{R}} \cdot 100 \qquad (1)$$

Table 1 - Acquisition parameters used in this work.

Acquisition parameter	Value
Input voltage	±12 V
Current injection time	1 s
V-delay (Vdly)	580 ms
M-delay (Mdly)	40 ms
Total integration time ($\Sigma_j \Delta T_j$)	880 ms
Sampling method	Semi-log
Number of IP windows (n)	20

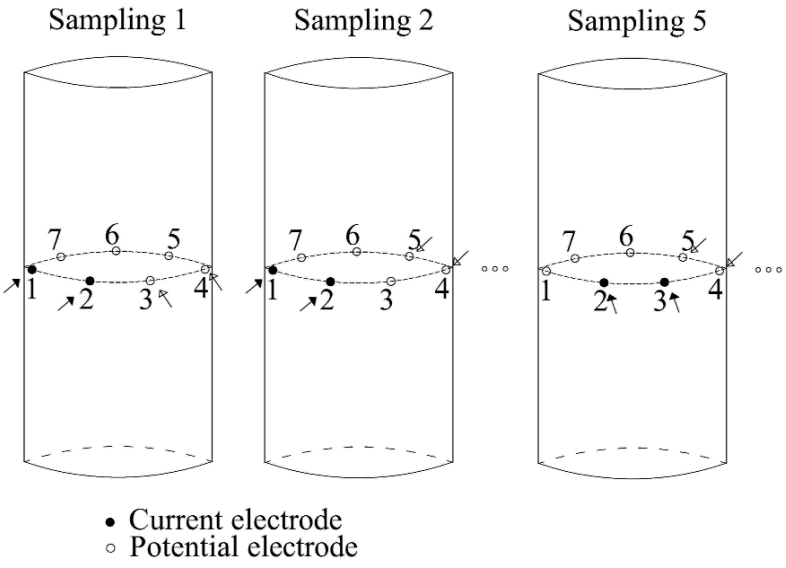

Fig. 4 - A seven-electrode configuration and dipole-dipole adjacent pattern for ERT and IP laboratory surveys.

where $\overline{R}$ is the average between R_i and R_{-i}.

On the other hand, using a DC source in a water filled sample, no charge accumulation should be displayed and any non zero chargeability measurement represents an error. Therefore, chargeability values are represented directly, with no reciprocal correlation (La Brecque and Daily, 2008).

For a single IP window, one defines apparent chargeability M_j (in mV/V), referring to Table 1, as follows:

$$M_j = \frac{\int_{\Delta T_j} V dt}{V_{MN} \cdot \Delta T_j} \cdot 1000 \tag{2}$$

where V_{MN} is the measured voltage on potential electrodes before the current cut off, V the sampled voltage after the current cut off and ΔT_j the single IP window. Both resistance and chargeability measurements are taken into account only after a delay time (Vdly and Mdly), as shown in Fig. 4.

Therefore, the four-electrode chargeability measurement (M_i) is:

$$M_i = \frac{\sum_{j=1}^{n} M_j \Delta T_j}{\sum_{j=1}^{n} \Delta T_j}. \tag{3}$$

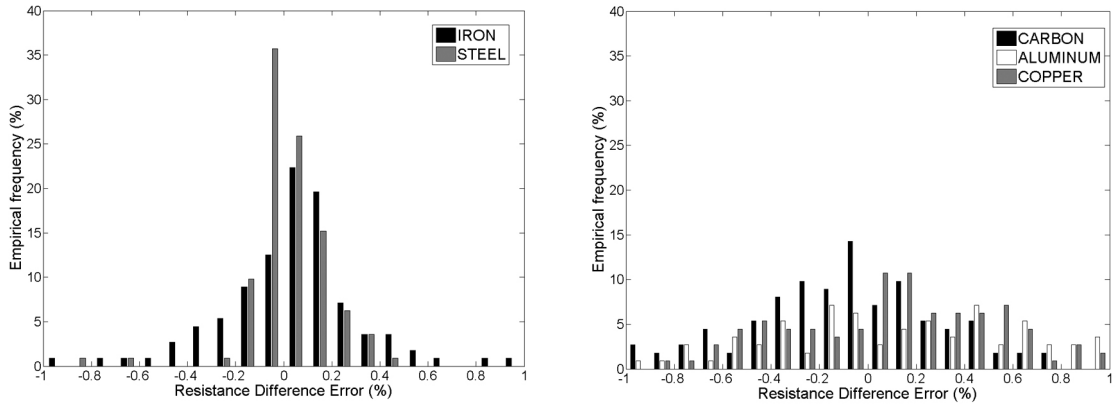

Fig. 5 - *RDE* empirical frequency for iron and steel (left), carbon, aluminium and copper (right).

3. Electrode performances

The statistical analysis has been summarized, for each data set, by histograms of the empirical frequency distributions of *RDE* (Fig. 5) and chargeability (Fig. 6), by a box-plot representation (Tukey, 1977) (Fig. 7) and by statistical indexes (Table 2 and Fig. 8).

The recovered data set are subdivided into 20 classes, from -1 to 1 (% or mV/V), and empirical frequency histograms (percentage ratio between the number of times the event occurred and the total number of events) are displayed. Figs. 5 and 6 show clearly that steel (best performance) and iron outperform carbon, aluminium and copper, both for resistance and for chargeability measurements, since more than 80% of samples are located between ±0.2% (resistance) and ±0.4 mV/V (chargeability). On the other hand, carbon, aluminium and copper presents flattened histograms, with appreciable empirical frequencies also for higher *RDE* and chargeability values.

In addition to this, a box-plot representation (Tukey, 1977) is useful to understand the contribution

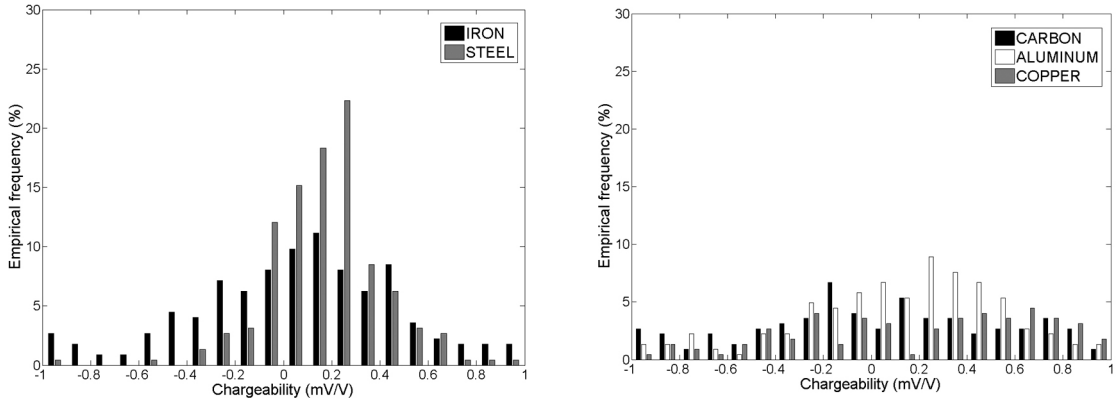

Fig. 6 - Chargeability empirical frequency for iron and steel (left), carbon, aluminium and copper (right).

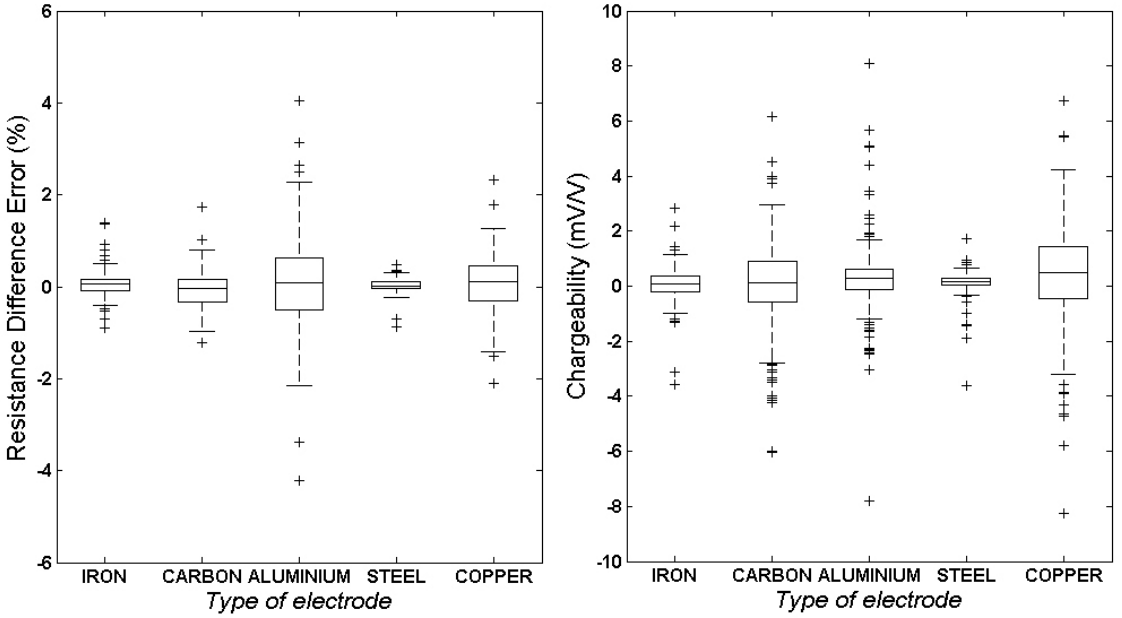

Fig. 7 - Box plots of *RDE* (left) and chargeability (right).

of the outliers within the data set and to display error bars for each material. The box width in Fig. 7 (interval between solid lines) is the Inter-Quartile Range (*IQR*), defined as follows:

$$IQR = Q_3 - Q_1 \tag{4}$$

where Q_1 and Q_3 are the lower (cuts off lowest 25% of data) and the upper (cuts off lowest 75% of data) quartiles of the empirical data set.

Any data not included between the dashed lines (the so-called whiskers) is plotted as an outlier (cross point). Whiskers are extended from Q_1−1.5*IQR* to Q_3+1.5*IQR*.

Table 2 - Mean (m), standard deviation (s) and (*IQR*) empirical values for *RDE* and chargeability measurements over the five materials employed as electrodes.

	RDE (%)			Chargeability (mV/V)		
Material	m	s	*IQR*	m	s	*IQR*
Steel	0.02	0.17	0.15	0.14	0.41	0.27
Iron	0.06	0.33	0.25	0.07	0.63	0.61
Carbon	-0.07	0.44	0.49	0.06	1.61	1.49
Copper	0.07	0.65	0.77	0.34	1.90	1.88
Aluminium	0.00	1.27	1.13	0.35	1.51	0.75

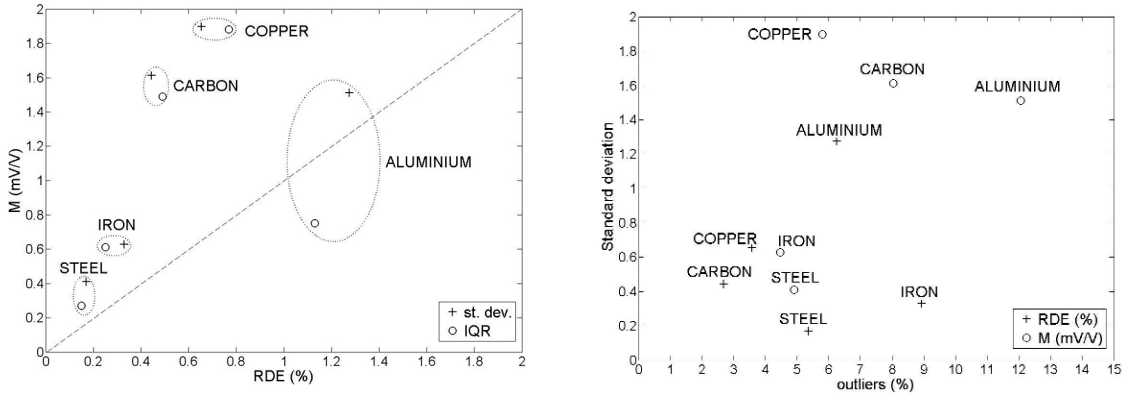

Fig. 8 - *RDE* vs. chargeability for the five electrode materials in water (left). Standard deviation (cross points) and *IQR* (circles) are represented together with the 1:1 dashed line. Correlation between the standard deviations [resistance cross points) and chargeability (circles)] and the percentage of outliers determined through box-plots (right).

Steel and iron electrodes have thin boxes, short whiskers and few outliers both for resistance and for chargeability plots, demonstrating high reliability for DC electrical measurements. As expected, aluminium has poor resistive characteristics (large box and long whiskers), although capacitive performances are affected by a remarkable presence of outliers (Fig. 8). Carbon and copper performances are quite satisfactory for resistance, while chargeability errors are the largest among the five materials.

The graphical and numerical representations of the most important statistical parameters (mean, standard deviation and *IQR*) have validated the previous analysis (Table 2 and Fig. 8). In particular, carbon and copper seem to be suitable for resistance measurements, steel has almost the same response for *RDE* and *M* (because of its location near the 1:1 line), while aluminium response is more uncertain and affected by outliers (Fig. 8).

Afterwards, previous results are compared (Table 3) to those by La Brecque and Daily (2008). Since they used AC sources, we made a comparison only with their lowest frequency (0.2 Hz)

Table 3 - Comparison between standard deviation empirical values for *RDE* and chargeability measurements recovered in this work (*s - DDC*) and after La Brecque and Daily (2008) (*s - LBD*). Only the lowest frequency (0.2 Hz) of La Brecque and Daily (2008) results is considered.

	RDE (%)		Chargeability (mV/V)	
Material	*s - LBD* AC-0.2 Hz	*s - DDC* DC	*s - LBD* AC-0.2 Hz	*s - DDC* DC
Steel	0.14	0.17	0.14	0.41
Iron	0.07	0.33	0.13	0.63
Carbon	0.42	0.44	0.57	1.61
Copper	0.24	0.65	0.24	1.90
Aluminium	0.88	1.27	2.35	1.51

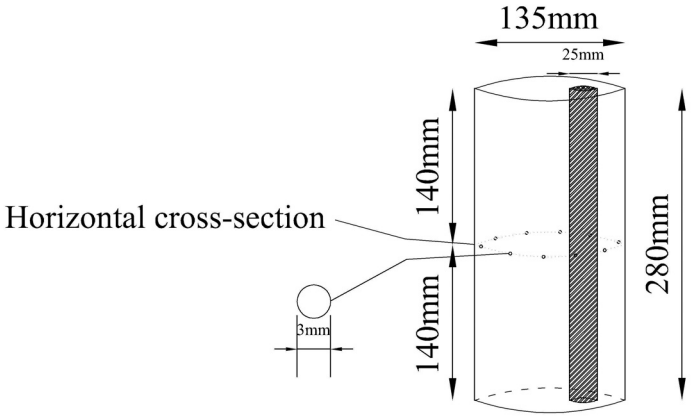

Fig. 9 - Synthetic model used to evaluate angular resolution.

data. Standard deviations recovered for *RDE* (*s - DDC)* are closer to La Brecque and Daily (2008) results (*s - LBD*). Although there are small differences in the two data sets, the main part of the evidence remains the same, as steel and iron are the best electrodes, copper and carbon suitable for resistance and aluminium the worst among the five materials. Chargeability standard deviations are greater for four of the five materials analyzed, probably because of the sensitivity of chargeability measurements to the particular working conditions and to the acquisition parameters employed.

4. Electrode configurations

The number of electrodes employed (angular resolution) are considered by performing four different inversions for 7, 10, 15 and 20 electrode configurations on the synthetic model described in Fig. 9.

The model is made of a resistive cylinder (ρ = 100 Ω·m, diameter ϕ = 135 mm), with a conductive (ρ_a = 10 Ω·m, ϕ_a = 25 mm) inclusion having a distance from the centre of 30 mm (Fig. 9). We use the finite element Matlab© code by Vauhkonen *et al.* (2001) to solve the resistivity forward problem, the Oldenburg and Li (1994) linear formulation for chargeability modelling, and a Gauss-Newton Occam's inversion (Loke and Barker, 1996) to invert resistivity and chargeability recovered data. The inversion results, presented in Fig. 10, show the important influence of the angular resolution on the inverse solution. In fact, a 7-electrode configuration is not able to reconstruct the inclusion (Figs. 10c and 10d), whereas the final models obtained employing 20 electrodes (Figs. 10e and 10f) are in good agreement with the true ones. According to Wheeler *et al.* (2002) and Adler *et al.* (2009) one may define some figures of merit to assess the resolution achieved by different configurations. Firstly, we calculate the number of elements in the finite element mesh (*x* and *y* respectively for resistivity and chargeability) to be assigned to the inclusion, as follows:

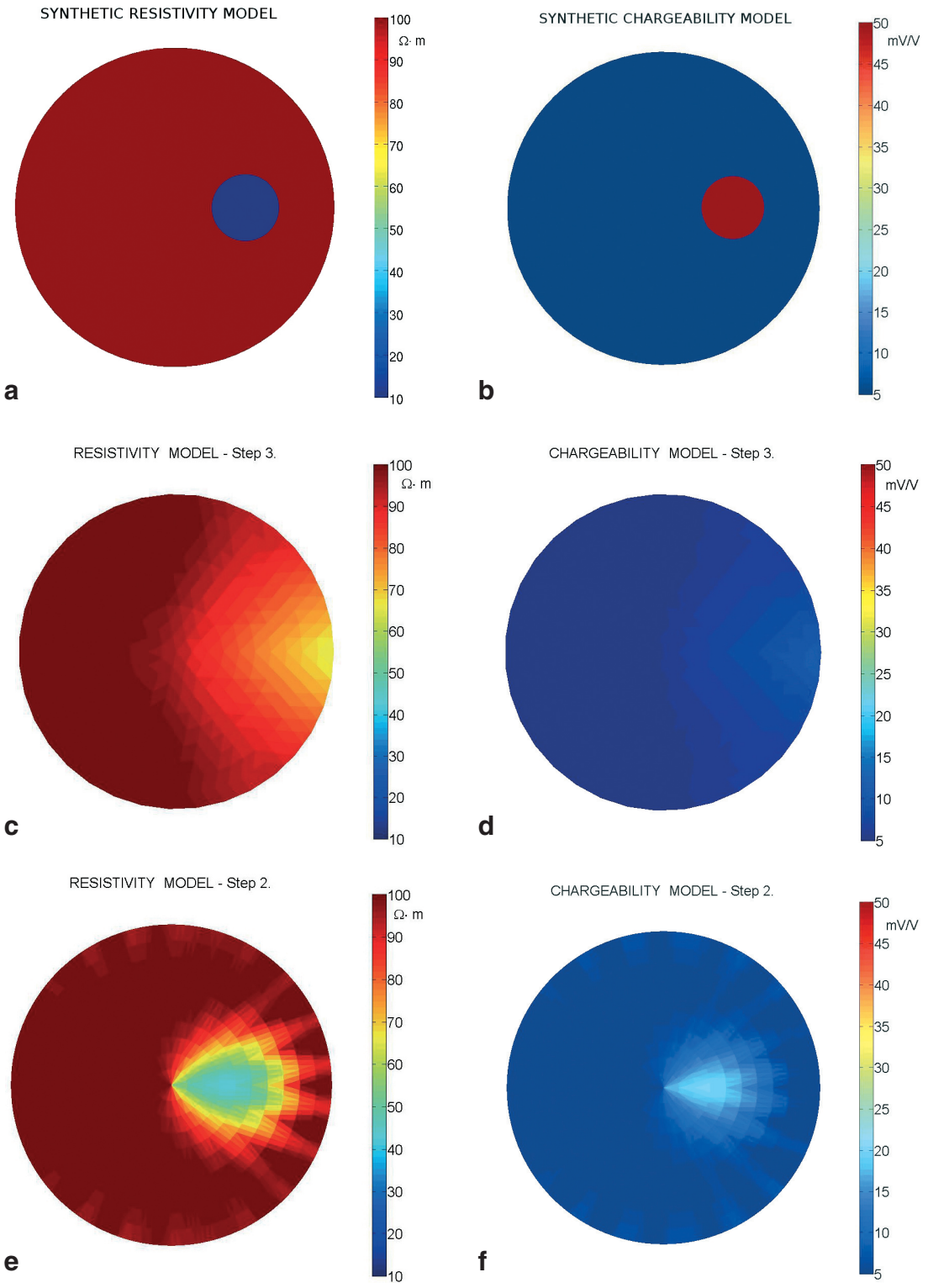

Fig. 10 - Resistivity and chargeability inverted models from synthetic data (only 7 and 20 electrode configurations are represented for the sake of simplicity). Resistivity and chargeability initial (a, b) and reconstructed models for 7 (c, d) and 20 (e, f) electrode configurations (respectively 3rd and 2nd iteration).

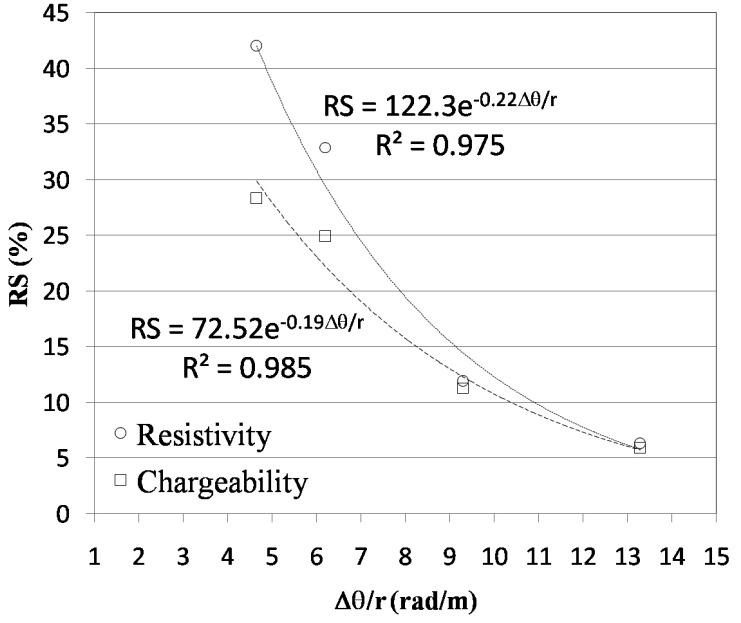

Fig. 11 - Percentage resolution (*RS*) vs. $\Delta\theta/r$ ratio, for resistivity (circle) and chargeability (square) models. Exponential type regressions are represented in dashed and dotted lines, respectively.

$$x_k = \begin{cases} 1 & \text{if } \rho_k < 1.5 \cdot \min(\rho_k) \\ 0 & \text{otherwise} \end{cases}, \quad y_k = \begin{cases} 1 & \text{if } M_k > 0.5 \max(M_k) \\ 0 & \text{otherwise} \end{cases} \quad k = 1,2,...,N \qquad (5)$$

where N is the number of elements.

We modify the multiplication factor by Adler *et al.* (2009) (0.5 instead of 0.25) to better evaluate the inhomogeneous results coming from different configurations.

Then, we introduce the resolution *RS* as the ratio between the number of elements (belonging to the inclusion) within the initial (Figs. 10a and 10b) and the final (Figs. 10c, 10d, 10e, and 10f) models:

$$RS(\rho) = \frac{\sum_k x_k^{init}}{\sum_k x_k^{final}}, \quad RS(M) = \frac{\sum_k y_k^{init}}{\sum_k y_k^{final}}. \qquad (6)$$

RS can vary within the (0,∞) range, as the inversion can provide an under-resolved model (*RS* close to zero) or an over-resolved one (*RS* > 1). The optimum *RS* value is 1.

The relationship between *RS* and $\Delta\theta/r$ (ratio between the incremental angle $\Delta\theta=2\pi/L$ and the radius r) can give us some information for the optimum number of electrodes to be employed in electrical laboratory surveys (Fig. 11). *RS* decreases exponentially passing from 4 to 13 rad/m (from 20 to 7 electrode configurations) and the data set is well-fitted (R^2=0.975 and 0.985).

5. Conclusions

Errors due to electrode materials, investigated by a DC device, are in good agreement with the previous work developed at laboratory scale (La Brecque and Daily, 2008). In particular, steel and iron perform well both for resistance and chargeability measurements, although steel has provided the best performance, almost uncontaminated by outliers and with an uniform response for *RDE* and *M*. Carbon and copper are suitable for resistance (few outliers and small standard deviations) but not recommended for IP. Aluminium does not have a satisfactory resistive and reactive behaviour, as seen after La Brecque and Daily (2008). Results for resistivity are comparable to those by La Bracque and Daily (2008), even though standard deviations are slightly higher. Chargeability is more sensitive to the particular working conditions and to the configuration used for the acquisition. Although chargeability errors recovered by La Brecque and Daily (2008) are smaller, the order of magnitude remains the same, with the same evidence for the performance of the electrodes.

In addition to this, an appropriate angular resolution of the cylindrical sample is strictly recommended, because of its importance for the correct resolution of the physical anomalies. In fact, resolution decreases exponentially with an increase of the $\Delta\theta/r$ ratio which represents the number of electrodes. As a result we underline the importance of an a priori analysis of errors due to electrodes, in order to calibrate laboratory surveys and to control the inversion algorithm.

Acknowledgments. This work is part of a PRIN financing, developed in cooperation with the University of Cagliari, the University of Palermo and the CNR-Milan. The authors wish to thank M. Cercato (Università "La Sapienza" di Roma) for his scientific contribution and F. Pugliese (Università "La Sapienza" di Roma) for his technical support during the laboratory surveys.

REFERENCES

Acar Y.B., Gale R.J., Alshawabkeh A.N., Marks R.B., Puppala W., Bricka M. and Parker R; 1995: *Electrokinetic remediation: basics and technology status.* Journal of Hazardous Materials, **40**, 117-137.

Adler A., Arnold J.H., Bayford R., Borsic A., Brown B., Dixon P., Faes T.J.C., Frerich I., Gagnon H., Gärber Y., Grychtol B., Hahn G., Lionheart W.R.B., Malik A., Patterson R.P., Stocks J., Tizzard A., Weiler N. and Wolf G.K.; 2009: *GREIT: a unified approach to 2D linear EIT reconstruction of lung images.* Physiological Measurement, **30**, 35–55.

Cardarelli E. and Di Filippo G.; 2009: *Electrical resistivity and induced polarization tomography in identifying the plume of chlorinated hydrocarbons in sedimentary formation: a case study in Rho (Milan - Italy).* Waste Management & Research, **27**, 595–602.

Dahlin T.; 2000: *Short note on electrode charge-up effects in DC resistivity data acquisition using multi-electrode arrays.* Geophysical Prospecting, **48**, 181-187.

Dahlin T., Leroux V. and Nissen J.; 2002: *Measuring techniques in induced polarisation imaging.* Journal of Applied Geophysics, **50**, 279-298.

Hördt A., Blaschek R., Kemna A. and Zisser N.; 2007: *Hydraulic conductivity estimation from induced polarisation data at the field scale-the Krauthausen case history.* Journal of Applied Geophysics, **62**, 33–46.

La Brecque D. and Daily W.; 2008: *Assessment of measurement errors for galvanic-resistivity electrodes of different composition.* Geophysics, **73**, 55-64.

Loke M.H. and Barker R.; 1996: *Rapid least-squares inversion of apparent resistivity pseudo-sections by a quasi-Newton method.* Geophysical Prospecting, **44**, 131-152.

Oldenburg D.W. and Li Y.; 1994: *Inversion of induced polarization data.* Geophysics, **59**, 1327-1341.

Slater L.D. and Glaser D.R.; 2003: *Controls on induced polarization in sandy unconsolidated sediments and application to aquifer characterization.* Geophysics, **68**, 1547–1588.

Slater L.D., Choi J. and Wu Y.; 2005: *Electrical properties of iron-sand columns: implications for induced polarization investigation and performance monitoring of iron-wall barriers.* Geophysics, **70**, 87–94.

Titov K., Kemna A., Tarasov A. and Vereecken H.; 2004: *Induced polarization of unsaturated sands determined through time domain measurements.* Vadose Zone Journal, **3**, 1160–1168.

Tukey J.W.; 1977: *Exploratory data analysis.* Addison-Wesley, Reading, MA, 688 pp.

Vanhala H. and Soininen H.; 1995: *Laboratory technique for measurement of spectral induced polarization response of soil samples.* Geophysical Prospecting, **43**, 655–676.

Vauhkonen M., Lionheart W., Heikkinen L.M., Vauhkonen P.J. and Kaipio J.P.; 2001: *A MATLAB package for the EIDORS project to reconstruct two-dimensional EIT images.* Physiological Measurement, **22**, 107–111.

Weller A., Frangos W. and Seichter M.; 1999: *Three-dimensional inversion of induced polarization data from simulated waste.* Journal of Applied Geophysics, **41**, 31–47.

Wheeler J.L., Wang W. and Tang M.; 2002: *A comparison of methods for measurement of spatial resolution in two-dimensional circular EIT images.* Physiological Measurement, **23**, 169–176.

Corresponding author: Giorgio De Donno
D.I.C.E.A., Università La Sapienza
Via Eudossiana 18, 00184 Rome, Italy
Phone: +39 06 44585102; fax: +39 06 44585080; e-mail: giorgio.dedonno@uniroma1.it